# Accepted Manuscript

Title: Structural, optical and photocatalytic properties of zinc oxides obtained from spent alkaline batteries

Authors: María V. Gallegos, Francisca Aparicio, Miguel A. Peluso, Laura C. Damonte, Jorge E. Sambeth

Please cite this article as: Gallegos MV, Aparicio F, Peluso MA, Damonte LC, Sambeth JE, Structural, optical and photocatalytic properties of zinc oxides obtained from spent alkaline batteries, *Materials Research Bulletin* (2010), https://doi.org/10.1016/j.materresbull.2018.03.022

**Structural, optical and photocatalytic properties of zinc oxides obtained from spent alkaline batteries.**

María V. Gallegos[a], Francisca Aparicio[b], Miguel A. Peluso[a*], Laura C. Damonte[c] and Jorge E. Sambeth[a]

[a]*Centro de Investigación y Desarrollo en Ciencias Aplicadas "Dr. Jorge J. Ronco" (CINDECA, CONICET-FCE UNLP), 47 Nro 257, (1900) La Plata, Buenos Aires(Argentina)*
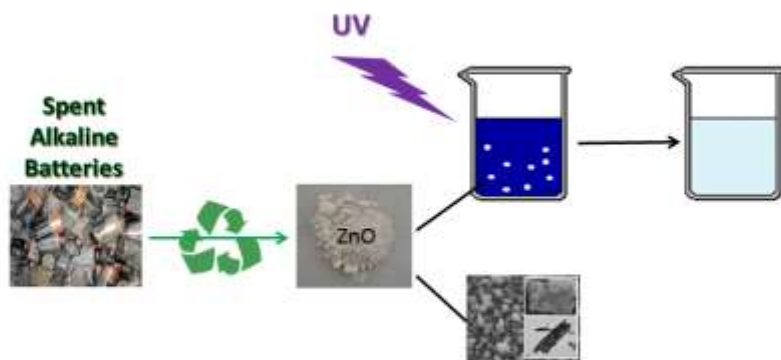
[b]*Instituto de Investigaciones Fisicoquímicas Teóricas y Aplicadas (INIFTA, CONICET-FCE UNLP) Diagonal 113 y 64, (1900) La Plata, Buenos Aires (Argentina)*

[c]*Instituto de Física La Plata (IFLP, CONICET – FCE UNLP) calle 49 y 115, (1900) La Plata, Buenos Aires (Argentina)*

*Corresponding author.

*E-mail address: apelu@quimica.unlp.edu.ar*

1

GRAPHICAL ABSTRACT



**Highlights**

- Zinc oxides were synthetized using spent alkaline batteries as raw materials.

- Both prepared samples present the wurzite structure and exhibits good optical properties.

 - The decrease in lattice parameters and the narrow band gap are associated with the

formation of oxygen vacancies.

- Recovered zinc oxides were active for photodegradation of methylene blue by UV irradiation.

- The photocatalytic was correlates to the bulk/surface defects ratio.

2

**ABSTRACT**

The structural, optical and photocatalytic properties of two zinc oxides prepared from spent alkaline batteries were analysed. After leaching the anode of alkaline batteries, zinc was precipitated from the leachate liquor by introducing oxalic acid (O-ZnO) or sodium carbonate (C-ZnO). The structure of ZnO samples were analysed by X-ray diffraction (XRD), scanning electron microscopy (SEM), transmission electron microscopy (TEM), $S_{BET}$, DRS-UV-Vis spectroscopy and positron annihilation lifetime spectroscopy (PALS). Both oxides present the ZnO wurzite structure and similar morphology. C-ZnO presents a cell lower lattice parameters and bang gap energy (2.99 eV) than O-ZnO (3.05 eV), possibly due to higher concentration of oxygen vacancies. The photocatalytic activity in the degradation of methylene blue (MB) of O-ZnO (achieving 70% MB degradation at 90 min) was superior to C-ZnO, due to its higher surface area and degree of crystallinity and lower bulk/surface defects ratio.

## 1. Introduction

ZnO is widely utilized as a semiconductor material due to its optical and electronic properties, low cost and low toxicity. The ZnO has a wide band gap of 3.4 eV and a large exciton binding energy of 60 meV at room temperature and these properties,

3

which are of considerable interest, take on added significance because they are related to applications such as optical and electronic devices, solar cells, gas sensors [1,2].

In order to obtain high-quality zinc oxide powders with fine particle size, narrow size distribution and special morphology, different techniques for preparing ZnO have been investigated such as sol-gel process, chemical coprecipitation, thermal decomposition, precipitation, microemulsion, etc. [3–5]. The different preparation methods are analyzed to create vacancies and defects, which are important parameters for electronic and optoelectronic applications. These synthetic routes require high temperature, sophisticated equipment and long time. For a large scale ZnO production, cheaper and quicker methods are needed [6].

According to Raj et al. [7], the synthesis of ZnO by using precipitation methods has a low cost, and the production of nano oxides with different sizes and shapes is reproducible.

In the last decades, the consumption of alkaline and Zn-C batteries has increased and the final disposal of spent batteries represents an increasing environmental problem. Batteries are dangerous waste, mainly due to the presence of heavy metals and, in many countries, alkaline and spent zinc-carbon batteries are still land filled or incinerated [8,9]. The anode of the alkaline batteries is composed of a mixture of zinc oxide and hydroxide and it could be a used as raw material for the synthesis of ZnO [10].

4

The recycling of zinc constitutes not only an environmental benefit, but also an economic one. According to the London Metal Exchange (LME), the zinc price in July 2017 was $2.8 / kg^{-1}$ (US).

Several processes have been proposed for the recycling of batteries, such as pyrometallurgical and hydrometallurgical methods. Hydrometallurgy has some benefits such as low cost requirements, possible recovery of leachants, and decrease of air pollution as there are no particles produced [11]. The experimental results indicated that in the case of Zn, the efficiency of the hydrometallurgical method is between 73% and 100% [12–14].

Synthetic dyes, widely used in the textile industry, are the major industrial pollutants and water contaminants [15,16]. In particular, methylene blue (MB) is a heterocyclic aromatic chemical compound that in drinking water causes several health damages.

Among different techniques employing for removing dyes from water, photocatalysis is a promising and emerging process for the purification of water [17–20].

Among different semiconductors used as photocatalysts, $TiO_2$ is the most widely oxide studied. Nevertheless, ZnO is considered an alternative of $TiO_2$ due its comparable band gap energy, lower cost and in some cases; the photoactivity of ZnO is superior to that of $TiO_2$ [21].

In this work we report a facile and eco-friendly method to fabricate zinc oxides, using a $Zn^{2+}$ solution as precursor obtained by dissolving the anode of spent alkaline batteries with a bio-generated sulfuric acid fabricated in our laboratory.

5

Structural and morphological properties of the oxides were investigated by powder x-ray diffraction (XRD) and scanning and transmission electron microscopy (SEM and TEM), the textural properties were analysed by means of nitrogen isotherms and the optical absorption properties by DRS-UV-visible absorption spectroscopy. Also, the study of the defects in the prepared ZnO were analysed by positron annihilation lifetime spectroscopy (PALS), which is one of the best techniques for probing vacancy defects in semiconductors [22,23]. PALS technique is a sensitive technique to correlate size effects and surface defects of nanoparticles with their electronic and optical properties. The photocatalytic properties of the prepared zinc oxides were investigated in the degradation of MB under UV light.

## 2. Materials and Methods

### 2.1 Synthesis of ZnO

Spent alkaline batteries of different sizes were collected. Batteries were manually dismantled and then, the anode and cathode were separated. The anodic paste, containing Zn, ZnO and KOH, was first washed with distilled water, dried at 120 ºC for 12 h and dissolved using a biogenerated sulfuric acid of pH= 0.8, for 2 h at 60 ºC using a solid/liquid ratio of 0.04 g mL$^{-1}$.

The production of the biogenerated sulfuric acid was described in a previous paper [24,25]. Briefly, *Acidithiobacillus thiooxidans* (*At*) bacteria produce an acid-reducing medium by oxidation of sulfur in an air-lift reactor. After leaching, zinc was

6

precipitated from the leachate liquor by introducing a precipitation agent. Then, 100 mL of $H_2C_2O_4$ 0.100M (Anhydrous 99%) or $Na_2CO_3$ 0.100M (Anhydrous 99%) was added to 100 mL of the solution containing $Zn^{2+}$, and the suspension was stirred at 30 ºC for 1 h. The product was filtered, washed with distilled water, and dried at 120 ºC for 24 h. Finally, the solid was calcined in air at 500 ºC for 2 h. The solids obtained were called O-ZnO (oxalic acid) and C-ZnO (sodium carbonate).

Fig. 1 shows the flow-sheet of the production of different zinc oxides from spent alkaline batteries.
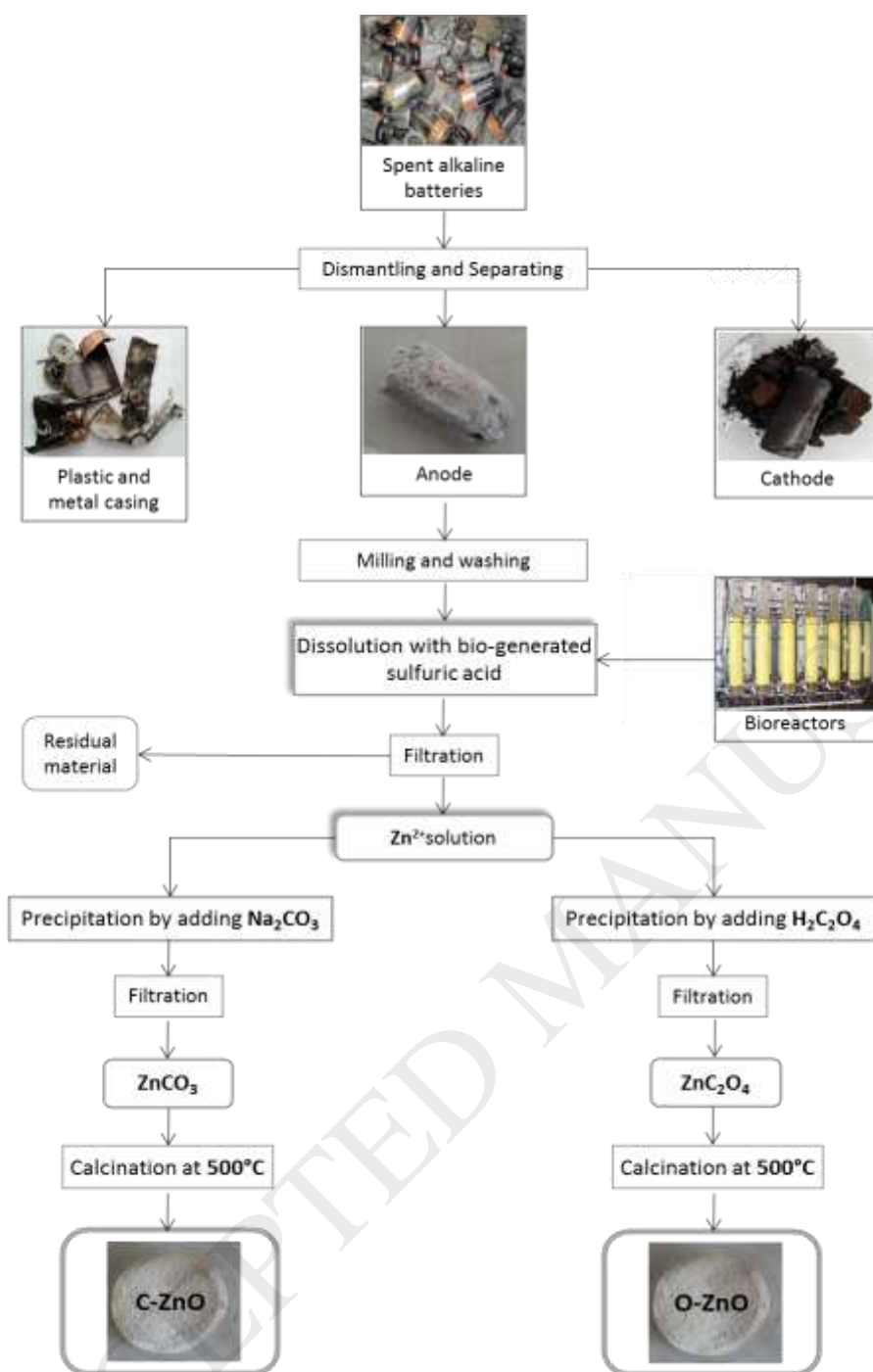
**Fig. 1.** Flow-sheet of the preparation of the recovered ZnO samples for spent alkaline batteries.

*2.2 Characterization*

The purity of the samples was measured by means of atomic absorption spectroscopy (AAS), in a Varian AA 240 spectrophotometer after dissolving the oxides in aqua regia. The samples were characterized by X-ray diffraction (XRD) method using a Philips diffractometer. The diffraction patterns were recorded at room temperature from 15 to 80º of 2θ using Cu Kα (λ = 1.5406 Å) radiation at 0.02º min$^{-1}$ scanning speed and a counting time of 2 s per step.

The BET specific areas were measured by $N_2$ adsorption at the liquid nitrogen temperature (77 K) in a Micromeritics Accusorb 2100 D sorptometer.

The surface morphology of the samples was studied using scanning electron microscopy (SEM) in a Philips SEM 505 microscope. TEM measurements were performed with a JEOL 100 CXII microscope operated at 100 kV.

Optical characterizations were carried out by measuring the diffuse reflectance spectroscopy. All spectra were taken in the range of 200-800 nm using a Perkin Elmer Lambda 35 UV-vis spectrophotometer with integrating sphere attachment and spectralon reflectance standard.

Positron annihilation lifetime measurements were collected in a conventional fast–fast coincidence system with two scintillator detectors (one $BaF_2$ and one plastic BURLE), which provided a time resolution (FWHM) of 260 ps using a $^{57}$Co source and previously setting the energy windows for $^{22}$Na. The radioactive source, $^{22}$NaCl (10 μCi), was deposited onto a Kapton foil (1.42 g cm$^{-3}$) and sandwiched between two

9

sample specimens. The source contribution and the response function were evaluated from a reference sample (Hf metal) using the RESOLUTION code [26]. The lifetime spectra (2–3x10$^6$ counts), acquired at room temperature, consist of various exponential decays:

$$n(t) = \sum_i I_i e^{(-\frac{t}{ti})} \quad (1)$$

the relative intensities $I_i$, normalized, being $\Sigma_i\ I_i = 1$. After background subtraction and convolution with the resolution function, the parameters that characterized each positron state, $\lambda_i$ annihilation rate ($\lambda_i = 1/\sigma_i$) and its intensity $I_i$, were obtained by means of POSITRONFIT program [26].

*2.3 Photocatalytic activity*

The photocatalytic activity of ZnO samples was investigated by degradation of methylene blue (MB) in an aqueous solution under UV irradiation. Experiments were carried out at room temperature under stirring in a RPR-100 Rayonet reactor equipped with 8RPR-3500 lamps with emission centered at $\lambda = 350$ nm.

20 mg of ZnO sample powder was mixed in 200 ml of 5 ppm aqueous MB solution. In degradation experiments, prior to irradiation, the aqueous solution was stirred continuously in the dark for 30 min to ensure adsorption/desorption equilibrium. The equilibrium concentration of MB was used as the initial value for the

photodecomposition processes. The decomposition of methylene blue was monitored at different times by measuring the absorbance of 5 mL aliquot solution using UV–vis spectrophotometer (at 665 nm) in liquid cuvette configuration with deionized water as reference.

## 3. Results and Discussion

### 3.1 Structural and morphological characterization

The component of the anodic paste, metallic zinc and zinc oxide can be fully leached by sulfuric acid media according to the following equations:

$$Zn + H_2SO_4 \rightarrow Zn^{2+} + SO_4^{2-} + H_2 \qquad (2)$$

$$ZnO + H_2SO_4 \rightarrow Zn^{2+} + SO_4^{2-} + H_2O \qquad (3)$$
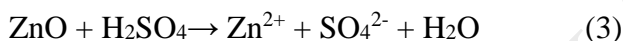
After leaching, a 0.4 M $Zn^{2+}$ solution was obtained. Two solids were prepared by precipitation of the $Zn^{2+}$ from the leached solution with $Na_2CO_3$ or $H_2C_2O_4$, and further calcination.

EDS analysis showed that the samples obtained after precipitation the $Zn^{2+}$ present in the leacheate liquor, O-ZnO and C-ZnO, contain 2.6 and 4.0 % w/w of sulfur, respectively. No manganese was detected in the samples.

The X-ray diffraction (XRD) patterns of the recovered zinc oxides are shown in Fig. 2. In both samples, C-ZnO and O-ZnO, all the diffraction peaks observed where those

11

corresponding to the planes (100), (002), (101), (102), (110), (103), (200), (112), (201) and (202) of the ZnO wurtzite phase (JCPDF # 36-1451). No other diffraction peaks are observed, indicating the completely transformation of the precursors into pure ZnO.
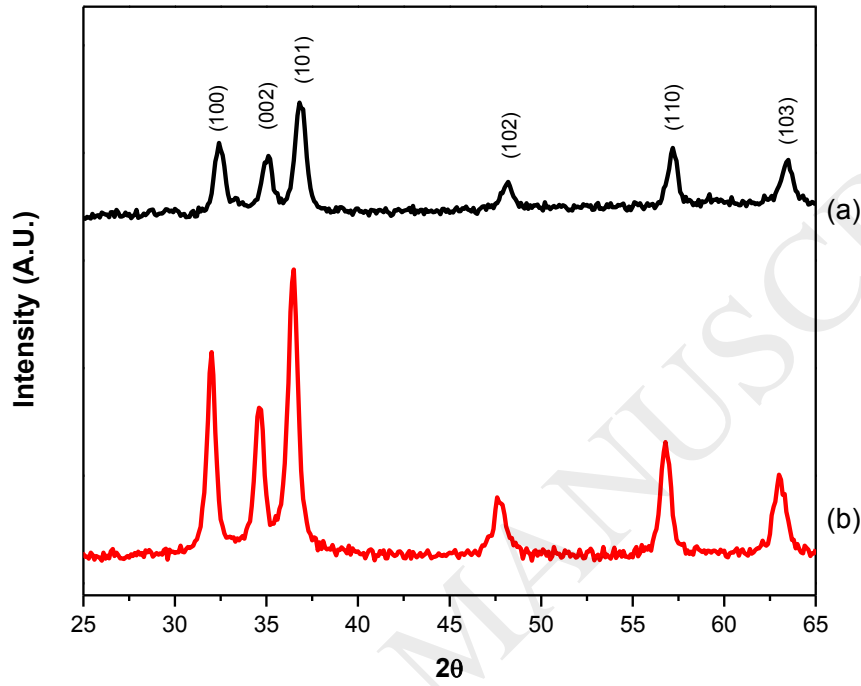


**Fig. 2.** X-ray diffraction patterns of the ZnO samples: (a) C-ZnO and (b) O-ZnO.

The intensity of the peak assigned to the (101) plane of the O-ZnO is higher than that of C-ZnO, indicating that the last sample has a lower degree of crystallinity [27,28].

The average crystal size (D) of the samples was estimated using the Scherrer formula:

$$D = \frac{0.9\lambda}{\beta\cos\theta} \quad (4)$$

12

where λ is the X-ray wavelength, θ is Bragg's diffraction angle and β is the angular line width of half maximum intensity of the diffraction peak corresponding to plane (101). The crystallite sizes calculated using Eq. (4) were 13 and 15 nm for C-ZnO and O-ZnO, respectively.

The lattice parameters obtained from Rietveld refinements are listed in Table 1. The values obtained are lower than those of lattice constants 3.249 Å and 5.206 Å of wurzite ZnO (JCPDF # 36-1451). Furthermore, it can be seen that the representative peak of the (101) plane in the diffraction patterns of the recovered oxides slightly shifts to higher 2θ values compared to the pure ZnO (36.2º) possibly due to the reduction in the lattice parameters. According to Dutta et al. [29] the change in peak position is consequence of the different kind of structural defects such as oxygen and zinc vacancies. Additionally, Li et al. [30], suggested that the oxygen vacancies reduce the c-parameter (the defects in the prepared ZnO samples will be discussed in the Section 3.3).

**Table 1.** XRD peak position and crystallite size of the studied ZnO samples.

| Sample | (1 0 1) Peak position (º) | FWHM | XRD crystallite size (nm) | β | a=b (Å) | c (Å) | c/a |
|---|---|---|---|---|---|---|---|
| **O-ZnO** | 36.4 | 0.5782 +/- 0.0038 | 15.1 +/- 0.1 | 0.6 | 3.20 | 5.17 | 1.61 |
| **C-ZnO** | 36.7 | 0.6849 +/- 0.0034 | 12.8 +/- 0.06 | 0.7 | 3.18 | 5.15 | 1.62 |

13

The SEM study (Fig. 3a and 3d) revealed that both C-ZnO and O-ZnO solids have platelet-shape morphology. According to different authors [7,31], the formation of platelets is due to the inhibition of the polar (001) face by sorption of $SO_4^{2-}$ anion, which consists of dipoles of positively charged $Zn^{2+}$ and negatively charged $O^{2-}$.

The TEM image of the samples (Fig. 3b and 3e) showed the formation of spherical shaped particles with the diameter of about 20 nm in both oxides, C-ZnO and O-ZnO, consistent with XRD results. Similar morphologies observed by TEM were reported by Ahmad et al. [16] over ZnO nanoparticles.

The $N_2$ adsorption/desorption isotherms of the prepared zinc oxides are presented in Fig. 4. The $N_2$ adsorption/desorption isotherms are all type IV isotherm, accompanied by a type H3 hysteresis loop, according to the IUPAC classifications, which correspond to material with mesoporous structure.
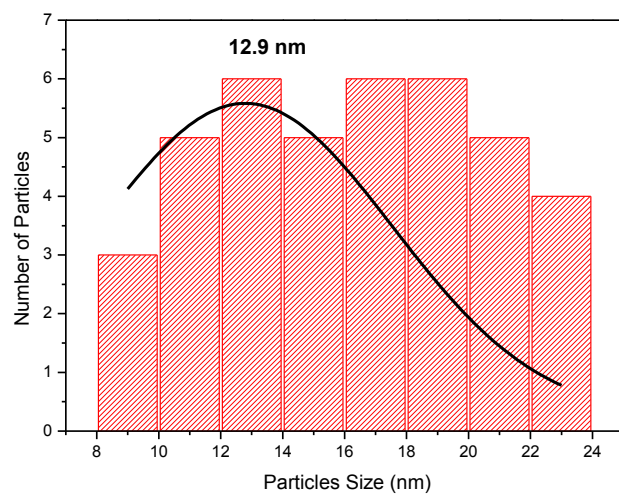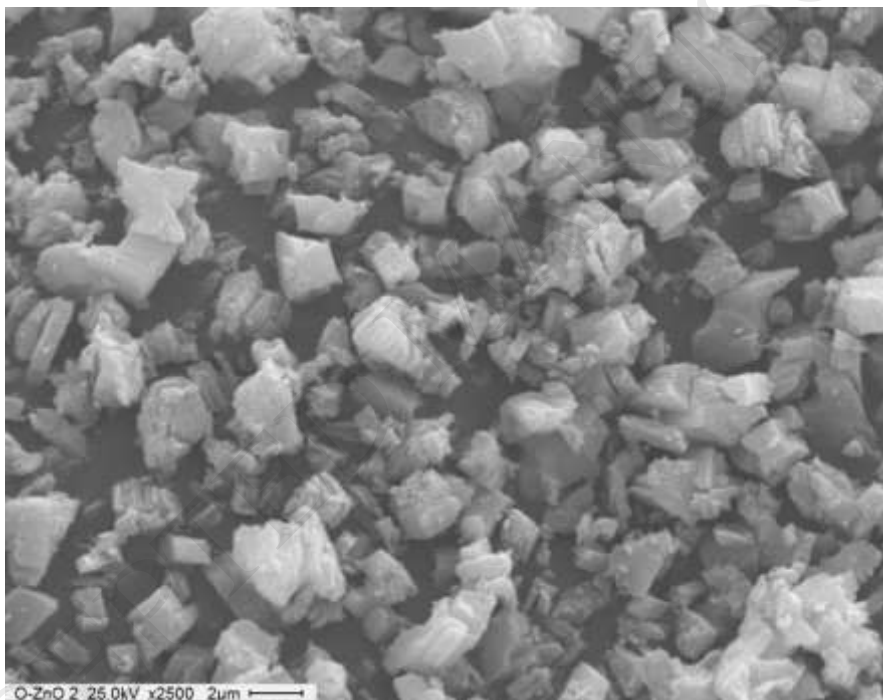
(a)



(b)

15
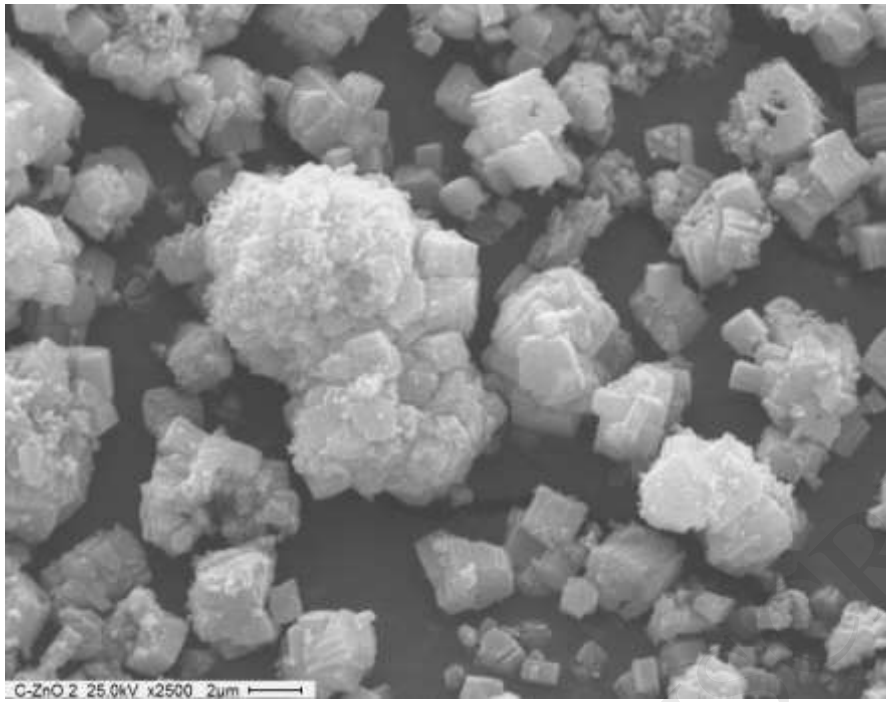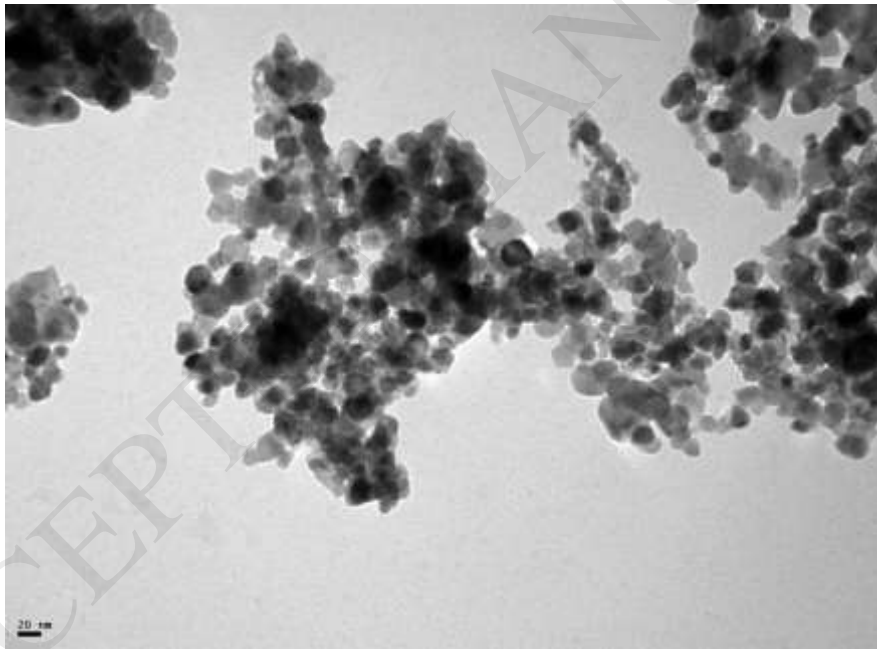
(c)



(d)
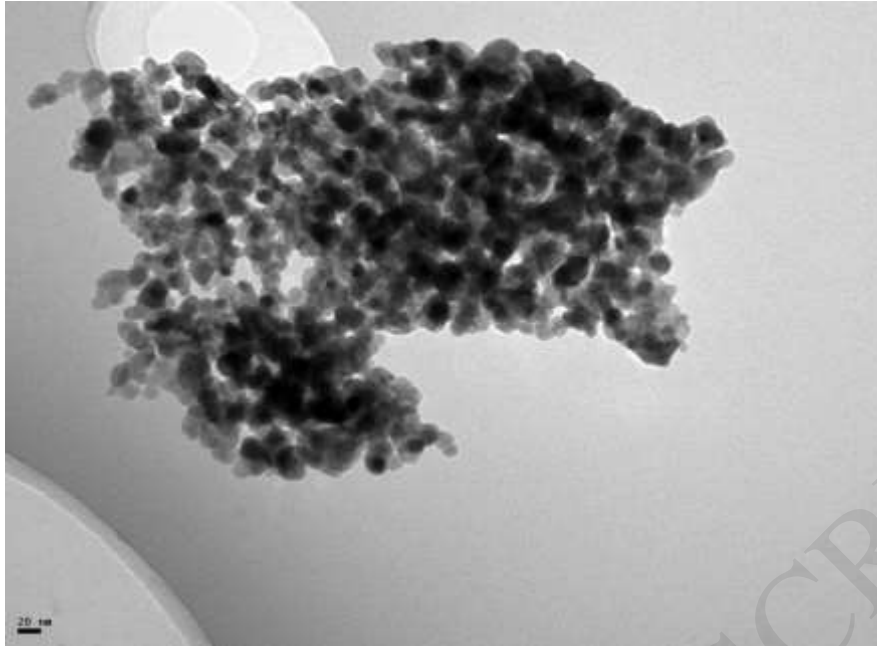
(e)
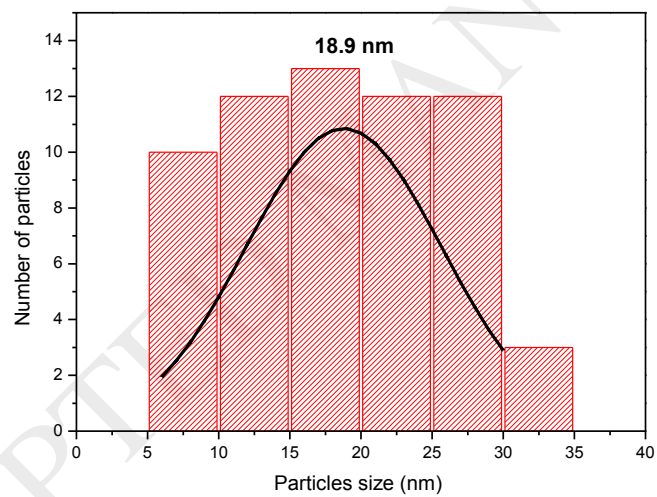


(f)

**Fig. 3.** SEM images, TEM micrographs and size distribution of (a,b,c) C-ZnO and (d,e,f) O-ZnO.
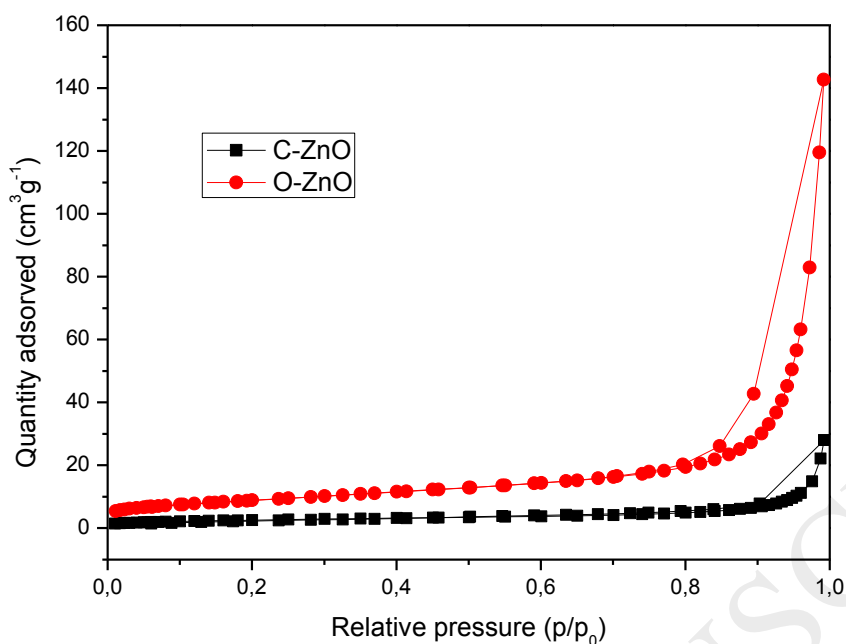
**Fig. 4.** Nitrogen adsorption-desorption isotherms of zinc oxide samples.

The BET surface area and average pore volume of the samples are shown in Table 2. Compared with other ZnO reported in bibliography [27] obtained also by precipitation with oxalic acid (17-22 $m^2g^{-1}$), the surface area of the ZnO prepared in this work by precipitation with oxalic acid is higher.

### 3.2 Optical characterization

Optical characterization was carried out by measuring the diffuse reflectance spectroscopy. The absorption spectra showed in Fig. 5 is characterized by broad and

18

strong absorptions profile in the UV region of electromagnetic spectrum, characteristic of the band edge absorption of wurtzite ZnO [32].

**Table 2.** Textural properties of the zinc oxides.

| Sample | $S_{BET}$ ($m^2g^{-1}$) | $V_p$ ($cm^3g^{-1}$) | Dp (A) | $E_g$ (eV) |
|--------|------|------|-----|------|
| **O-ZnO** | 31 | 0.22 | 191 | 3.05 |
| **C-ZnO** | 9 | 0.05 | 181 | 2.99 |

The absorption edge of C–ZnO shifted to higher wavelengths compared to O-ZnO. According to Tauc−Mott, the photon energy ($E_f$) dependence of the absorption coefficient ($\alpha$) can be described as [33]:

$$\alpha E_f = B(E_f - E_g)^n \quad (5)$$

where B is a constant, $E_g$ is the band gap of the material and n is an index that characterizes the optical absorption process (for direct band gap semiconductor material such as ZnO, n = ½). Therefore, the band gap energy of the as-prepared ZnO powders can be estimated from a plot of $(\alpha E_f)^2$ versus $E_f$, extrapolating the linear part of the graph (Fig. 6) until it meets the x-axis.

19

Calculated $E_g$ values for C-ZnO and O-ZnO were 3.05 eV and 2.99 eV, respectively. Band gap of different ZnO reported in literature measured by Tauc procedure are in the range 3.09-3.24 eV [32,34–36].
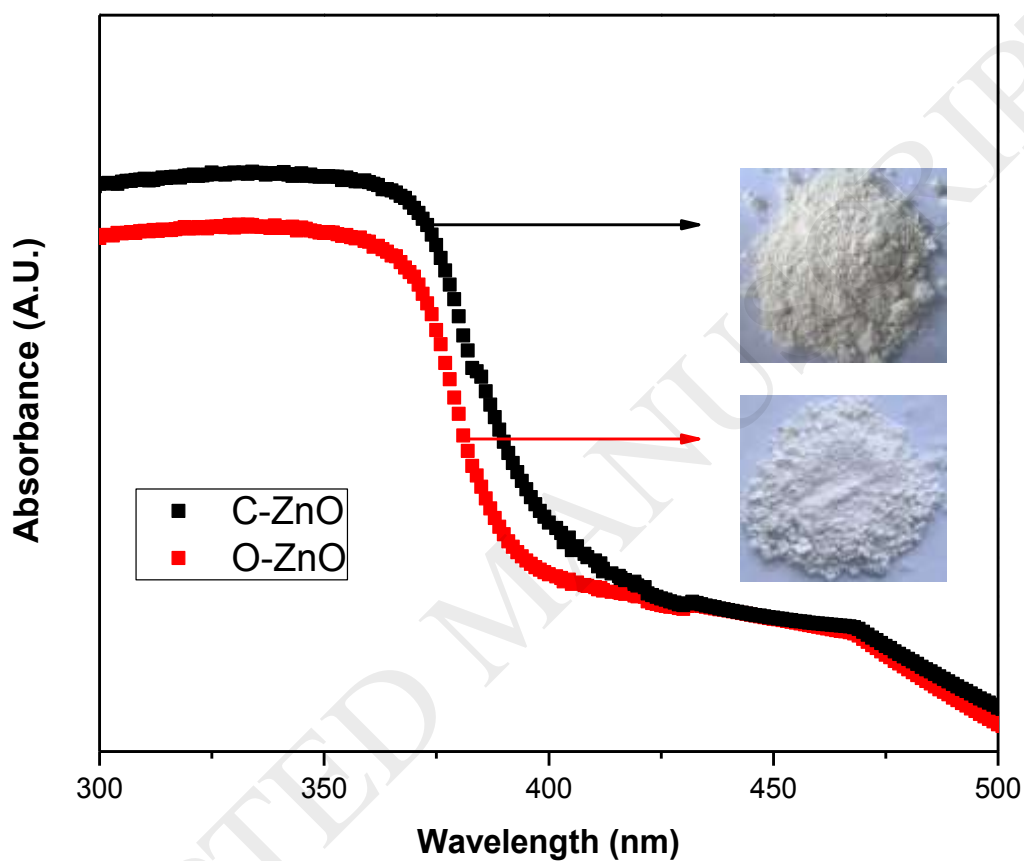


**Fig. 5.** Optical absorbance spectra for the different ZnO samples.

It is reported that the red shift in the UV-vis spectra is due to size difference and formation of crystal defects, and the greater the red shift in the UV–vis spectra, the

higher the concentration of defects [37]. Additionally, Peng et al. [36] indicate that the presence of defect sites contributes also to a decrease in the band gap values. Furthermore, Bhatia and Nerma [38] show that the variation in band gap is associated with structural parameter, grain size, and induced defects.

The color of the samples (inset of Fig. 5) could also be associated with the band gap energy. The light-yellow color of C-ZnO sample is in accord with its narrow band gap, in agreement with Peng et al. [36] and Wolski et al [27].
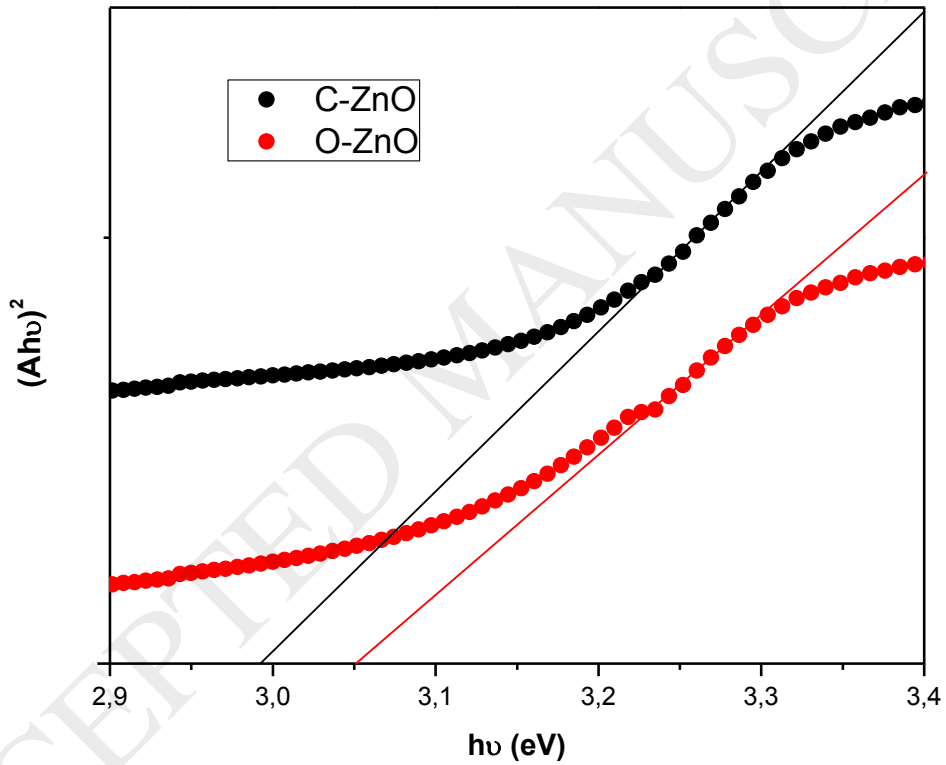


**Fig. 6.** Plot $(\alpha E_f)^2$ vs $E_f$ for the ZnO samples.

Apart from the band gap, the band tail parameter ($E_0$) can give important hint towards the disorder present in the samples. $E_0$ is defined as

$$\alpha(E_f) = \alpha_0 \exp\left( E_f \Big/ E_0 \right) \quad (6)$$

where $\alpha_0$ is a constant and $E_0$ is the band tail parameter.

The band tail region (lower energy part just below the band edge, $E_g$) of the ZnO samples is shown in Fig. 7. $E_0$ has been estimated from the reciprocal of the slope by fitting the linear part of the ln ($\alpha$) vs. $E_f$ curves (just below $E_g$) of the respective ZnO samples.

The obtained $E_0$ value for C-ZnO and O-ZnO were 670 and 250 meV, respectively. The enhancement of $E_0$ indicates the increase of disorder in the system. In addition, an increase of $E_0$ is due to an increase in the number of oxygen vacancies [29]. These observations are in agreement with the results of XRD on the samples.
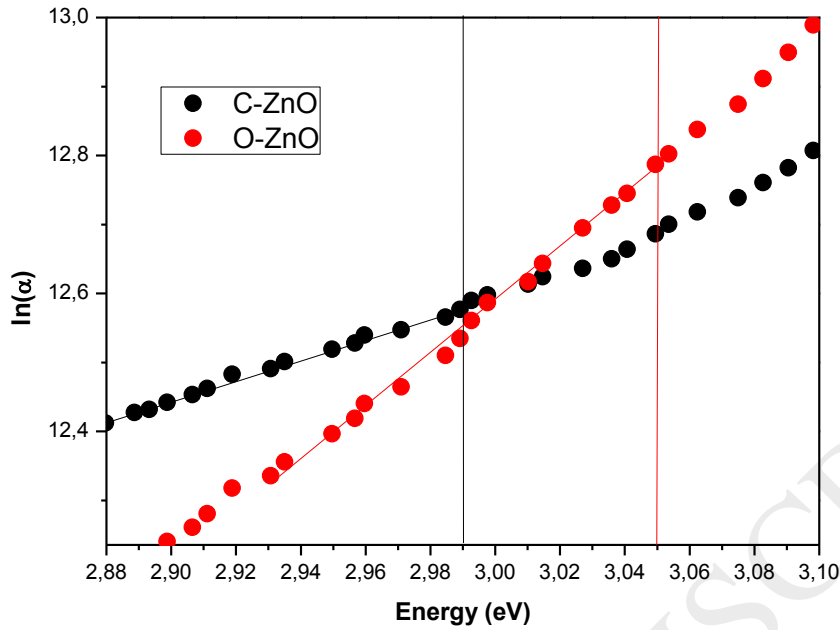
**Fig.7.** Plots of ln($\alpha$) with photon energy, where $\alpha$ is the absorption coefficient. The vertical lines represent the band gap value (red line O-ZnO and black line C-ZnO).

*3.3 Positron annihilation spectroscopy analysis*

The defects in the prepared ZnO samples were studied by positron annihilation lifetime measurements. The positron lifetime spectra were decomposed into three exponential decays without source correction, each one characterized by a positron lifetime $\tau_i$ of intensity $I_i$. Three components are choose based on probable positron annihilation sites in nanocrystalline systems and also for getting a $\chi^2$ close to 1.0 [39].

23

In semiconductors, the presence of two lifetimes is a usual feature, as predicted by the two-state trapping model. The first one corresponding to free positrons annihilated in the interstitial region and the second one senses trapped positrons at defects [40].

Table 3 listed the resulting annihilation positron parameters for the studied samples. The third and longer lifetime corresponds to ortho-positronium annihilation formed in large voids present in the material. The intensity of this third component in all the studied samples is low so it has not been considered in the following discussion.

The bulk lifetime of ZnO ($\tau_b$) represents the annihilations from a perfect crystal and has been reported different values for $\tau_b$ ranging from 151 ps to 180 ps [41]. In general, if there is only one type of defects, $\tau_1$ will be less than $\tau_b$. Nevertheless, $\tau_1$ could be higher than $\tau_b$ if there are two or more types of defects.

The high first lifetime value for C-ZnO is probably due to the presence of new positron traps whose associated lifetime value are similar and cannot be distinguished. In nanocrystalline materials, monovacancies or grain boundaries frequently act as positron annihilation sites with similar values to bulk lifetime [22].

The second lifetime $\tau_2$ is sensing positrons trapped at larger size defects such as vacancy clusters (nanovoids) or at intersection interfaces (i.e. triple lines).

The relation $\tau_2/\tau_b$ is used to characterize the defect. The values obtained for C-ZnO and O-ZnO using $\tau_b = 180$ ps, were 2.2 and 2.12, respectively. It is known that for monovacancies this relation is around 1.5 [42, 43], therefore, the higher value for this

24

parameter constitutes other evidence that the second lifetime represents positron annihilation at large vacancy clusters in the prepared samples.

**Table 3. Positron Lifetime and Relative intensities of the ZnO samples.**

| Sample | $\tau_1$ (ps) | $\tau_2$ (ps) | $\tau_3$ (ps) | $I_1$ (%) | $I_2$ (%) | $I_3$ (%) | $I_1/I_2$ |
|--------|---------------|---------------|---------------|-----------|-----------|-----------|-----------|
| **C-ZnO** | 199 | 396 | 1572 | 41 | 53 | 6 | 0.77 |
| **O-ZnO** | 171 | 383 | 1634 | 29 | 67 | 4 | 0.43 |

Apart from positron lifetimes, its relative intensity provides information on the relative concentration of defects. The intensity ratio ($I_1/I_2$) is higher in C-ZnO than in O-ZnO. This indicates that C-ZnO has more monovacancies and fewer high size defects (divacancies or agglomeration of vacancies) than O-ZnO. In other words, C-ZnO has a higher relative concentration ratio of bulk defects-surface defects ($C_b/C_s$). Positron lifetimes originating from oxygen vacancies ($V_O$) and zinc vacancies ($V_{Zn}$) in ZnO have been experimentally found to be 180 ps and 230 ps, respectively. In view of this and our results, it may be concluded that the dominant defects in C-ZnO samples are $V_O$, while O-ZnO has a greater number of larger size defects clustered near the grain boundary that acts as positron traps. The present results are in good agreement with those reported by Dutta et al. [29] for ZnO nanoparticles obtained by mechanical milling.

*3.4 Photocatalytic activity*

25

The photocatalytic properties of the as prepared zinc oxides were evaluated in the photodegradation of MB under UV light. The photodegradation efficiency as a function of time was represented as $C/C_0$, where $C_0$ and $C$ are the initial and actual concentration of MB, respectively.

The photocatalytic degradation profiles of MB over ZnO samples are presented in Fig. 8a. In the absence of photocatalyst, MB exhibit poor degradation, reflecting the high stability of MB under UV irradiation. In the presence of O-ZnO about 70% degradation of MB was observed at 90 minutes, while in the case of C-ZnO, at the same time the 50 % degradation of MB was observed.

Furthermore, the degradation kinetics of the MB solution was also investigated, and the results are shown in Fig. 8b. The degradation rates of MB solution match well with pseudo-first- order reaction according to the simplified Langmuir-Hinshelwood model:

$$\ln\left(C/C_0\right) = -kt \quad (7)$$

where $k$ is the reaction rate constant ($min^{-1}$) and $C_0$ and $C$ are the initial and actual concentration of MB at time t, respectively. O-ZnO shows the highest photocatalytic activity with a rate constant of 0.0061 $min^{-1}$, which is larger than that of C-ZnO (0.0036 $min^{-1}$).

It is accepted that the photocatalytic activity depends on the recombination rate of photo-generated electrons (e$^-$) and holes (h). If the e-h separation is low, the rate of

26

recombination is high and electrons and holes recombine instead of reaching the surface. Thus increasing the e-h separation conducts to and enhanced photocatalytic activity. There are several that affect the rate of charge carrier recombination such as the surface area, the crystalline structure, degree of crystallinity and the size and shape of the photocatalyst particles [35,44].

Both prepared zinc oxides, O-ZnO and C-ZnO, presents the same crystalline structure, with rather similar particle size, but O-ZnO presents a higher surface area and a higher degree of crystallinity than C-ZnO.
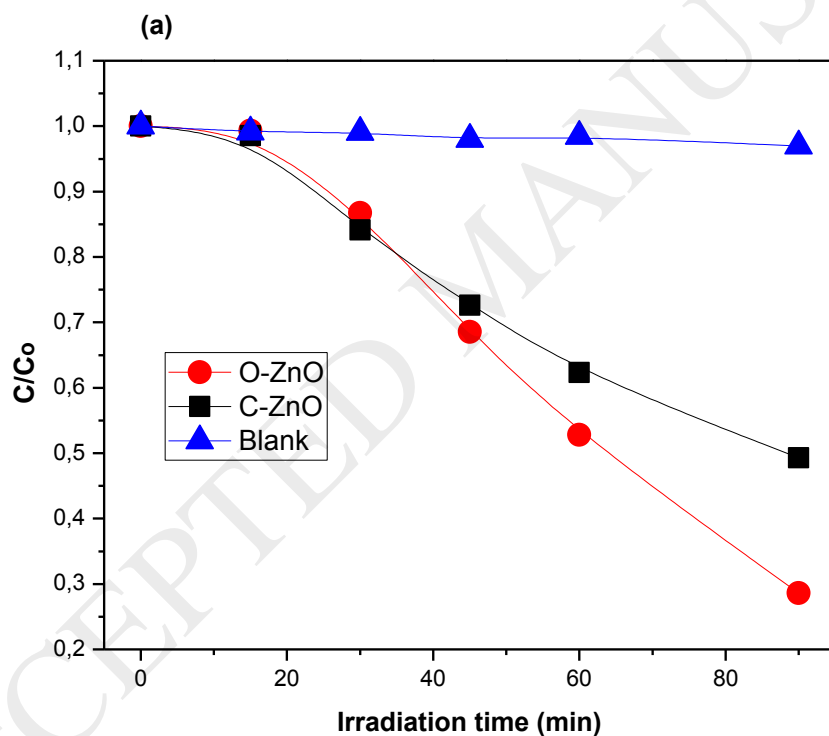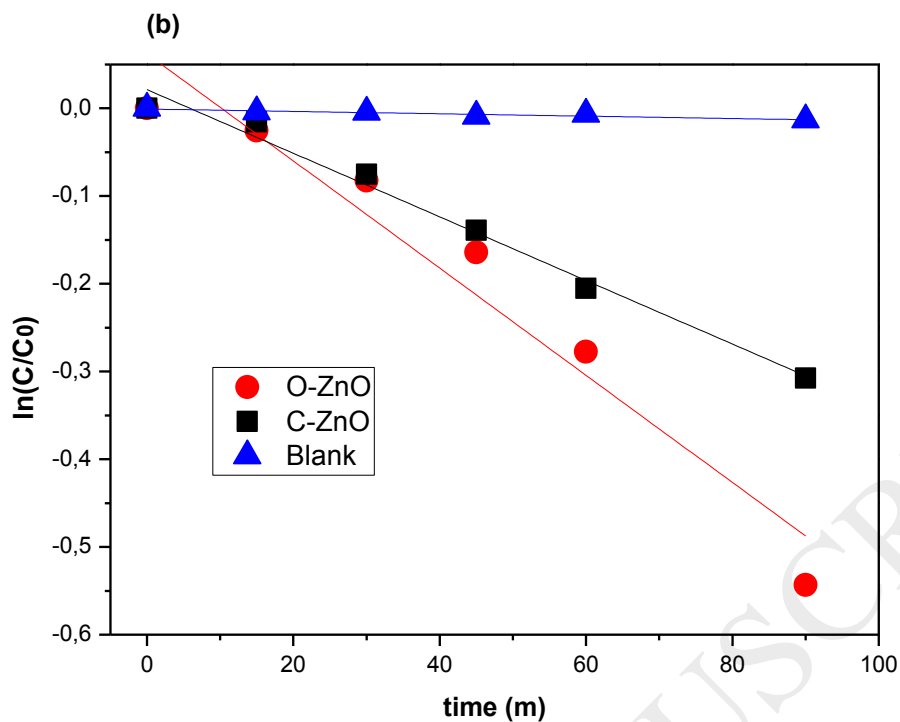
**Fig. 8.** (a) Photocatalytic degradation (C/C$_0$) and (b) degradation kinetics of the MB solution over C-ZnO and O-ZnO with increasing UV-light irradiation time.

The higher photocatalytic conversion of MB exposure to UV light of O-ZnO sample could be associated to its higher surface area and crystallinity.

Additionally, it was reported that a decrease in the $C_b/C_s$ ratio leads to an increase in the e-h separation efficiency [45–47]. In our work, O-ZnO with a lower $C_b/C_s$ ratio than C-ZnO, exhibits the highest photoactivity in the degradation of MB.

28

Finally, as the oxygen vacancies results in band gap narrowing and strong absorption of visible light, the as-prepared zinc oxides could be potential materials for degradation of contaminants under visible light and solar energy conversion devices.


## 4. Conclusions

Spent alkaline batteries can be harmful for the environment, and could be a source of materials. Battery recycling therefore promises significant environmental and economic benefits. The preparation of zinc oxides from spent alkaline batteries and their use in environmental applications has been proposed in this work.

ZnO nanoparticles were synthesized by dissolving the anode of spent alkaline batteries and further precipitation with sodium carbonate and oxalic acid and calcination in air at 500 ºC. The prepared zinc oxides were uses as photocatalysts for MB degradation under Uv light. Both prepared samples present the wurzite structure and exhibits good optical properties. The decrease in lattice parameters and the narrow band gap are associated with the formation of oxygen vacancies.

The results of photocatalytic experiments showed that the photocatalytic activity increased with the increase of surface area, the high degree of crystallinity and the lower ratio of bulk defects-surface defects.

Spent alkaline batteries could be used as raw materials for the preparation of effective photocatalyst materials and potential solar energy devices.

29

## Acknowledgements

## Reference

[1]  L.E. Greene, B.D. Yuhas, M. Law, D. Zitoun, P. Yang, Solution-Grown Zinc Oxide Nanowires, Inorg. Chem. 45 (2006) 7535–7543. doi:10.1021/ic0601900.

[2]  K. Arshak, E. Moore, G.M. Lyons, J. Harris, S. Clifford, A review of gas sensors employed in electronic nose applications, Sens. Rev. 24 (2004) 181–198. doi:10.1108/02602280410525977.

[3]  L.C. Damonte, L.A. Mendoza Zélis, B. Marí Soucase, M.A. Hernández Fenollosa, Nanoparticles of ZnO obtained by mechanical milling, Powder Technol. 148 (2004) 15–19. doi:10.1016/j.powtec.2004.09.014.

[4]  B. Sarkar, A.V. Daware, P. Gupta, K.K. Krishnani, S. Baruah, S. Bhattacharjee, Nanoscale wide-band semiconductors for photocatalytic remediation of aquatic pollution, Environ. Sci. Pollut. Res. 24 (2017). doi:10.1007/s11356-017-0252-3.

30

[5]     A. Balcha, O.P. Yadav, T. Dey, Photocatalytic degradation of methylene blue
        dye by zinc oxide nanoparticles obtained from precipitation and sol-gel methods,
        Environ. Sci. Pollut. Res. 23 (2016) 25485–25493. doi:10.1007/s11356-016-
        7750-6.

[6]     R. Rusdi, A.A. Rahman, N.S. Mohamed, N. Kamarudin, N. Kamarulzaman,
        Preparation and band gap energies of ZnO nanotubes, nanorods and spherical
        nanostructures, Powder Technol. 210 (2011) 18–22.
        doi:10.1016/j.powtec.2011.02.005.

[7]     C.J. Raj, R.K. Joshi, K.B.R. Varma, Synthesis from zinc oxalate, growth
        mechanism and optical properties of ZnO nano/micro structures, Cryst. Res.
        Technol. 46 (2011) 1181–1188. doi:10.1002/crat.201100201.

[8]     Greenpeace Argentina, y BateriasGestion de Residuos de Pilas y Baterias,
        Buenos Aires, 2010.
        http://www.greenpeace.org/argentina/Global/argentina/report/2010/7/informe-
        gestion-pilas-baterias.pdf.

[9]     Dirección de Residuos Peligrosos Dirección Nacional de Control Ambiental
        Subsecretaría de Control y Fiscalización Ambiental y Prevención de la
        Contaminación Pilas en Argentina, Buenos Aires, 2010. www.ambiente.org.ar.

31

[10]  C. Sardá, G. Escalante, I. García-Díaz, F.A. López, P. Fernández, Luminescence and gas-sensing properties of ZnO obtained from the recycling of alkaline batteries, J. Mater. Sci. (2017). doi:10.1007/s10853-017-1667-4.

[11]  E. Sayilgan, T. Kukrer, G. Civelekoglu, F. Ferella,  A. Akcil, F. Veglio, M. Kitis, A review of technologies for the recovery of metals from spent alkaline and zinc–carbon batteries, Hydrometallurgy. 97 (2009) 158–166. doi:10.1016/j.hydromet.2009.02.008.

[12]  C.C.B. Martha De Souza, D. Corrêa De Oliveira, J.A.S. Tenório, Characterization of used alkaline batteries powder and analysis of zinc recovery by acid leaching, J. Power Sources. 103 (2001) 120–126. doi:10.1016/S0378-7753(01)00850-3.

[13]  I. De Michelis, F. Ferella, E. Karakaya, F. Beolchini, F. Vegliò, Recovery of zinc and manganese from alkaline and zinc-carbon spent batteries, J. Power Sources. 172 (2007) 975–983. doi:10.1016/j.jpowsour.2007.04.092.

[14]  Y. Li, G. Xi, The dissolution mechanism of cathodic active materials of spent Zn-Mn batteries in HCl, J. Hazard. Mater. 127 (2005) 244–248. doi:10.1016/j.jhazmat.2005.07.024.

[15] N. Modirshahla, M.A. Behnajady, F. Ghanbary, Decolorization and
mineralization of C.I. Acid Yellow 23 by Fenton and photo-Fenton processes,
Dye. Pigment. 73 (2007) 305–310. doi:10.1016/J.DYEPIG.2006.01.002.

[16] C.C. Chen, Degradation pathways of ethyl violet by photocatalytic reaction with
ZnO dispersions, J. Mol. Catal. A Chem. 264 (2007) 82–92.
doi:10.1016/j.molcata.2006.09.013.

[17] W.L.W. Lee, C.S. Lu, H.P. Lin, J.Y. Chen, C.C. Chen, Photocatalytic
degradation of ethyl violet dye mediated by $TiO_2$ under an anaerobic condition, J.
Taiwan Inst. Chem. Eng. 45 (2014) 2469–2479. doi:10.1016/j.jtice.2014.04.025.

[18] W. Shen, Z. Li, H. Wang, Y. Liu, Q. Guo, Y. Zhang, Photocatalytic degradation
for methylene blue using zinc oxide prepared by codeposition and sol-gel
methods, J. Hazard. Mater. 152 (2008) 172–175.
doi:10.1016/j.jhazmat.2007.06.082.

[19] M. Thirumavalavan, F.M. Yang, J.F. Lee, Investigation of preparation conditions
and photocatalytic efficiency of nano ZnO using different polysaccharides,
Environ. Sci. Pollut. Res. 20 (2013) 5654–5664. doi:10.1007/s11356-013-1575-
3.

[20]  Z. Cai, Y. Sun, W. Liu, F. Pan, P. Sun, J. Fu, An overview of nanomaterials applied for removing dyes from wastewater, Environ. Sci. Pollut. Res. 24 (2017) 15882–15904. doi:10.1007/s11356-017-9003-8.

[21]  R.D.C. Soltani, A. Rezaee, A.R. Khataee, M. Safari, Photocatalytic process by immobilized carbon black/ZnO nanocomposite for dye removal from aqueous medium: Optimization by response surface methodology, J. Ind. Eng. Chem. 20 (2014) 1861–1868. doi:10.1016/j.jiec.2013.09.003.

[22]  S.K. Sharma, P.K. Pujari, K. Sudarshan, D. Dutta, M. Mahapatra, S. V. Godbole, O.D. Jayakumar, A.K. Tyagi, Positron annihilation studies in ZnO nanoparticles, Solid State Commun. 149 (2009) 550–554. doi:10.1016/j.ssc.2009.01.005.

[23]  J. Hoya, J.I. Laborde, L.C. Damonte, Structural characterization of mechanical milled ZnSe and ZnTe powders for photovoltaic devices, Int. J. Hydrogen Energy. 37 (2012) 14769–14772. doi:10.1016/j.ijhydene.2011.12.082.

[24]  M. V. Gallegos, L.R. Falco, M.A. Peluso, J.E. Sambeth, H.J. Thomas, Recovery of manganese oxides from spent alkaline and zinc-carbon batteries. An application as catalysts for VOCs elimination, Waste Manag. 33 (2013) 1483–1490. doi:10.1016/j.wasman.2013.03.006.

[25] L.R. Falco, A. Martinez, M. Di Nanno, H. Thomas, G. Curutchet, Study of a pilot plant for the recovery of metals from spent alkaline and zinc-carbon batteries with biological sulphuric acid and polythionate production,, Lat. Am. Appl. Res. 44 (2014) 123–129.

[26] P. Kirkegaard, N.J. Pedersen, M.M. Eldrup, PATFIT-88: A Data-Processing System for Positron Annihilation Spectra on Mainframe and Personal Computers, 1989.

[27] L. Wolski, J.E. Whitten, I. Sobczak, M. Ziolek, The effect of the preparation procedure on the morphology, texture and photocatalytic properties of ZnO, Mater. Res. Bull. 85 (2017) 35–46. doi:10.1016/j.materresbull.2016.08.027.

[28] M. Ahmad, E. Ahmed, W. Ahmed, A. Elhissi, Z.L.L. Hong, N.R.R. Khalid, Enhancing visible light responsive photocatalytic activity by decorating Mn-doped ZnO nanoparticles on graphene, Ceram. Int. 40 (2014) 10085–10097. doi:10.1016/j.ceramint.2014.03.184.

[29] S. Dutta, S. Chattopadhyay, A. Sarkar, M. Chakrabarti, D. Sanyal, D. Jana, Role of defects in tailoring structural, electrical and optical properties of ZnO, Prog. Mater. Sci. 54 (2009) 89–136. doi:10.1016/j.pmatsci.2008.07.002.

[30]   X. Li, Y. Wang, W. Liu, G. Jiang, C. Zhu, Study of oxygen vacancies' influence

on the lattice parameter in ZnO thin film, Mater. Lett. 85 (2012) 25-28.

doi:10.1016/j.matlet.2012.06.107.

[31]   E.A. Davis, N.F. Mott, Conduction in non-crystalline systems V. Conductivity,

optical absorptionand photoconductivity in amorphoussemiconductors,

Philosophical Magazine 22 (1970) 0903-0922.

[32]   R.M. Thankachan, N. Joy, J. Abraham, N. Kalarikkal, S. Thomas, O.S.

Oluwafemi, Enhanced photocatalytic performance of ZnO nanostructures

produced via a quick microwave assisted route for the degradation of rhodamine

in aqueous solution, Mater. Res. Bull. 85 (2017) 131–139.

doi:10.1016/j.materresbull.2016.09.009.

[33]   J. Tauc, Amorphous and Liquid Semiconductors, Springer US, Boston, MA,

1974. doi:10.1007/978-1-4615-8705-7.

[34]   V. Thi, B. Lee, Effective photocatalytic degradation of paracetamol using La-

doped ZnO photocatalyst under visible light irradiation, Mater. Res. Bull. 96

(2017) 171-182. doi:10.1016/j.materresbull.2017.04.028.

[35]   F. Sun, Z. Zhao, X. Qiao, F. Tan, W. Wang, Microwave synthesis and

photocatalytic activities of ZnO bipods with different aspect ratios, Mater. Res. Bull. 74 (2016) 367–373. doi:10.1016/j.materresbull.2015.10.054.

[36]    Y. Peng, Y. Wang, C. Qing-Guo, Z. Qing, W. An, Stable yellow ZnO mesocrystals with excellent visible light photocatalytic activity, CrystEngComm. 16 (2014) 7906–7913.

[37]    F. Aousgi, W. Dimassi, B. Bessais, M. Kanzari, Effect of substrate temperature on the structural, morphological, and optical properties of $Sb_2S_3$ thin films, Appl. Surf. Sci. 350 (2015) 19–24. doi:10.1016/j.apsusc.2015.01.126.

[38]    S. Bhatia, N. Verma, Photocatalytic activity of ZnO nanoparticles with optimization of defects, Mater. Res. Bull. 95 (2017) 468–476. doi:10.1016/j.materresbull.2017.08.019.

[39]    S. Ghosh, G.G. Khan, K. Mandal, S. Thapa, P.M.G. Nambissan, Positron annihilation studies of vacancy-type defects and room temperature ferromagnetism in chemically synthesized Li-doped ZnO nanocrystals, J. Alloys Compd. 590 (2014) 396–405. doi:10.1016/j.jallcom.2013.12.149.

[40]    P. Hautojärvi, C. Corbel, Positron Spectroscopy of Defects in Metals and Semiconductors, in: A. Dupasquier, A.P. Millis (Eds.), Positron Spectrosc.

Solids, Amsterdam, 1995: pp. 491–532. doi:10.3254/978-1-61499-211-0-491.

[41]  T. Ghoshal, S. Kar, S. Biswas, S.K. De, P.M.G. Nambissan, Vacancy-type defects and their evolution under Mn substitution in single crystalline ZnO nanocones studied by positron annihilation, J. Phys. Chem. C. 113 (2009) 3419–3425. doi:10.1021/jp805602f.

[42]  F. Tuomisto, A. Mycielski, K. Grasza, Vacancy defects in (Zn, Mn)O, Superlattices Microstruct. 42 (2007) 218–221. doi:10.1016/j.spmi.2007.04.071.

[43]  S. Chattopadhyay, S.K. Neogi, A. Sarkar, M.D. Mukadam, S.M. Yusuf, A. Banerjee, S. Bandyopadhyay, Defects induced ferromagnetism in Mn doped ZnO, J. Magn. Magn. Mater. 323 (2011) 363–368. doi:10.1016/j.jmmm.2010.09.042.

[44]  L. Du, Z. Long, H. Wen, W. Ge, Y. Zhou, J. Wang, (Ionic liquid)-derived morphology control of $Nb_2O_5$ materials and their photocatalytic properties, CrystEngComm. 16 (2014) 9096–9103. doi:10.1039/C4CE00987H.

[45]  M. Kong, Y. Li, X. Chen, T. Tian, P. Fang, F. Zheng, X. Zhao, Tuning the relative concentration ratio of bulk defects to surface defects in $TiO_2$ nanocrystals leads to high photocatalytic efficiency, J. Am. Chem. Soc. 133 (2011) 16414–

38

16417. doi:10.1021/ja207826q.

[46]   Y. Zheng, C. Chen, Y. Zhan, X. Lin, Q. Zheng, K. Wei, J. Zhu, Y. Zhu, Luminescence and Photocatalytic activity of ZnO Nanocrystals : Correlation between Structures and Properties, Inorg. Chem. 46 (2007) 6675–82. doi:10.1021/ic062394m.

[47]   X. Zhang, J. Qin, Y. Xue, P. Yu, B. Zhang, L. Wang, R. Liu, Effect of aspect ratio and surface defects on the photocatalytic activity of ZnO nanorods, Sci. Rep. 4 (2015) 4596. doi:10.1038/srep04596.

39